Energy-speed-accuracy relation in complex networks for biological discrimination

Felix Wong,[1,2] Ariel Amir,[1] and Jeremy Gunawardena[2,*]
[1]*School of Engineering and Applied Sciences, Harvard University, Cambridge, Massachusetts 02138, USA*
[2]*Department of Systems Biology, Harvard Medical School, Boston, Massachusetts 02115, USA*

(Received 15 August 2017; revised manuscript received 7 June 2018; published 30 July 2018)

Discriminating between correct and incorrect substrates is a core process in biology, but how is energy apportioned between the conflicting demands of accuracy (μ), speed (σ), and total entropy production rate (P)? Previous studies have focused on biochemical networks with simple structure or relied on simplifying kinetic assumptions. Here, we use the linear framework for timescale separation to analytically examine steady-state probabilities away from thermodynamic equilibrium for networks of arbitrary complexity. We also introduce a method of scaling parameters that is inspired by Hopfield's treatment of kinetic proofreading. Scaling allows asymptotic exploration of high-dimensional parameter spaces. We identify in this way a broad class of complex networks and scalings for which the quantity $\sigma \ln(\mu)/P$ remains asymptotically finite whenever accuracy improves from equilibrium, so that $\mu_{\mathrm{eq}}/\mu \to 0$. Scalings exist, however, even for Hopfield's original network, for which $\sigma \ln(\mu)/P$ is asymptotically infinite, illustrating the parametric complexity. Outside the asymptotic regime, numerical calculations suggest that, under more restrictive parametric assumptions, networks satisfy the bound, $\sigma \ln(\mu/\mu_{\mathrm{eq}})/P < 1$, and we discuss the biological implications for discrimination by ribosomes and DNA polymerase. The methods introduced here may be more broadly useful for analyzing complex networks that implement other forms of cellular information processing.

DOI: 10.1103/PhysRevE.98.012420

I. INTRODUCTION

In cellular information processing, a biochemical mechanism is coupled to an environment of signals and substrates and carries out tasks such as detection [1–5], amplification [6–8], discrimination [9–24], adaptation [25], searching [26], and learning [27–30]. As Hopfield pointed out in his seminal work on discrimination [9], systems operating at thermodynamic equilibrium have limited information processing capability and energy must be expended to do better [8,32].

We focus here on the widely studied task of discrimination between correct and incorrect substrates, an essential feature of many core biological processes. The accuracy of discrimination may have to be traded off against speed while energy remains a limiting resource [25,31]. How can energy be apportioned between such desirable properties as accuracy and speed and the inevitable dissipation of heat to the environment? Quantitative insights into this question can help us distill the principles underlying cellular information processing despite the pervasive complexity of the underlying molecular mechanisms.

Previous studies of discrimination have largely focused on particular systems, such as Hopfield's original proofreading mechanism [9,19,20], McKeithan's T-cell receptor mechanism [14,18], minimal feedback mechanisms [25], irreversible multistep mechanisms [23], or ladder mechanisms [12,15,16,21]. Murugan *et al.* analyzed general systems using simplifying assumptions about where energy is expended and showed how discriminatory regimes also depend on the topology of the mechanism [15,16]. Several studies have analyzed the relationship between energy expenditure and other properties away from thermodynamic equilibrium. These have often been limited to networks with simplifying assumptions [11–13,15,19–24] or have considered different questions in the context of kinetic proofreading [13,15,16,22–24,33,34]. The results in Refs. [17,25,35] show some formal similarities to those presented in this paper and these studies are reviewed further in the Discussion (Sec. IX).

One of the challenges in dealing with general systems away from thermodynamic equilibrium is that the steady-state probabilities can be complex algebraic functions of the parameters (see the Discussion) [8,32], which makes it difficult to identify any universal behavior. We address this issue here in two ways. First, we use a graph-based treatment of Markov processes called the "linear framework" [36], which allows steady-state probabilities to be analytically calculated for processes of arbitrary structure away from thermodynamic equilibrium (Secs. II and III). Second, we introduce a way of exploring parameter space by scaling the parameters. This idea is inspired by Hopfield's original analysis of kinetic proofreading, which we revisit here to point out certain subtleties that are not always appreciated (Sec. IV). The scaling method allows us to calculate the asymptotic behavior of steady-state properties of general systems, despite the difficulties arising from high-dimensional parameter spaces and algebraic complexity. In this way, we are able to exhibit a universal asymptotic relationship between energy, speed and accuracy for a broad class of discriminatory systems, without simplifying assumptions as to where energy is expended (Sec. VI). We further explore whether this asymptotic relationship also has significance for finite parameter values and for actual biological discrimination mechanisms (Sec. VIII).

*Electronic address: jeremy@hms.harvard.edu

 ©2018 American Physical Society

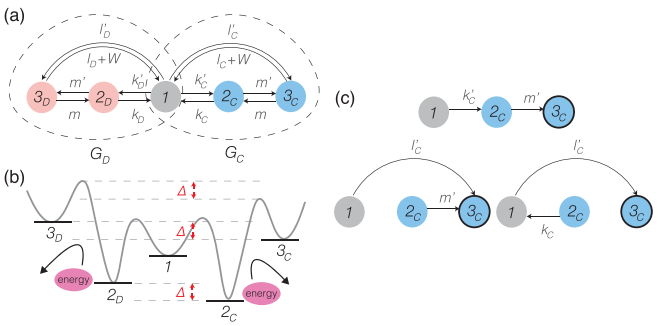

FIG. 1. The Hopfield mechanism and the linear framework. (a) Labeled, directed "butterfly" graph for the original Hopfield mechanism in Ref. [9], consisting of the subgraph G_D for the incorrect substrate D (within left-hand dashed circle) and the subgraph G_C for the correct substrate C (within right-hand dashed circle), which share the common vertex 1. Cyan and magenta denote correct and incorrect substrate binding, respectively. (b) Hypothetical energy landscape for the Hopfield mechanism showing where energy may be expended to drive the proofreading step with label m'. (c) The spanning trees of G_C rooted at 3_C (circled) are shown. A spanning tree is a subgraph which includes every vertex (spanning) and has no cycles when edge directions are ignored (tree); it is rooted at i if i is the only vertex with no outgoing edges. Any nonroot vertex has only a single outgoing edge. Using Eqs. (1) and (3), the trees shown here give the left-hand factor in the denominator of Eq. (4) and the remaining factors arise in a similar way.

II. THE LINEAR FRAMEWORK

The linear framework [36–38] is a graph-based interpretation of biochemical processes which has been used to analyze protein post-translational modification [39], covalent modification switches [40], and eukaryotic gene regulation [8,32]. In the stochastic setting considered here, the framework follows the treatment previously developed by Hill [41] and Schnakenberg [42]. A finite-state Markov process M is represented by a directed graph, G, with labeled edges and no self-loops [Fig. 1(a)], hereafter a "graph." The vertices $1, \ldots, n$, are interpreted as microstates and a labeled edge, $i \xrightarrow{a} j$, as a transition between microstates whose label, a, is the infinitesimal transition rate of the Markov process. The equations of motion are defined as if the edges are reactions under mass action kinetics, with the labels being the corresponding rates. This yields the master equation of the Markov process in the form $dp/dt = \mathcal{L}(G)p$, in which $p \in (\mathbb{R}_{\geqslant 0})^n$ is the vector of microstate probabilities and $\mathcal{L}(G)$ is the Laplacian matrix of G. For instance, for the subgraph G_C in Fig. 1(a),

$$\mathcal{L}(G_C) = \begin{pmatrix} -(k'_C + l'_C) & k_C & l_C + W \\ k'_C & -(k_C + m') & m \\ l'_C & m' & -(l_C + W + m) \end{pmatrix}.$$

Since probability is conserved, there is a conversation law, $\sum_i p_i(t) = 1$, where $p_i(t)$ is the probability that M is in microstate i at time t.

If the graph is strongly connected, so that any two vertices can be joined by a path of edges in the same direction, then there is a unique steady state up to a scalar multiple. A representative steady state, $\rho(G)$, can be calculated in terms of the labels by the matrix-tree theorem (MTT): if $\Theta_i(G)$ denotes the set of spanning trees rooted at i [Fig. 1(c)], then $\rho_i(G)$ is the sum of the product of the labels on the edges of each tree,

$$\rho_i(G) = \sum_{T \in \Theta_i(G)} \left(\prod_{j \xrightarrow{a} k \in T} a \right). \tag{1}$$

The steady-state probabilities are then

$$p_i^* = \left(\frac{\rho_i(G)}{\rho_1(G) + \cdots + \rho_n(G)} \right). \tag{2}$$

If the steady state is one of thermodynamic equilibrium, so that detailed balance is satisfied, then the framework gives the same result as equilibrium statistical mechanics, with the denominator in Eq. (2) being the partition function (up to a constant factor). However, Eq. (2) is also valid away from equilibrium.

In contrast to eigenvalues or determinants, the MTT gives the steady state analytically in terms of the labels [Eq. (1)]. This makes it feasible to undertake a mathematical analysis, without relying on numerical simulation, whose scope is necessarily more restricted. Substantial algebraic complexity can arise in Eq. (1) through the combinatorial explosion of enumerating spanning trees (Discussion) but, as we show here, with the appropriate mathematical language, it is possible to draw rigorous conclusions about structurally complex systems away from thermodynamic equilibrium. In particular, we exploit the fact that steady-state probabilities are rational functions in the labels, which allows us to determine asymptotic behaviors.

III. STEADY STATES OF A BUTTERFLY GRAPH

Discrimination typically requires a mechanism for choosing a correct substrate from among a pool of available substrates, as in DNA replication, in which DNA polymerase must choose at each step one correct deoxynucleoside triphosphate from among the four available (dATP, dGTP, dCTP, dTTP). We follow Hopfield in assuming a single correct substrate, C, and a single incorrect substrate, D, and describe this mechanism by a graph G [e.g., Fig. 1(a)] whose vertices represent the microstates of the discriminatory mechanism, such as DNA polymerase in the case of replication. This graph is naturally composed of two subgraphs, G_X ($X = C, D$), corresponding to the states in which substrate X is bound. G_C and G_D share a common vertex, but no edges, so that G has a butterfly shape.

We will denote such a butterfly graph $G = G_C \oplus_v G_D$, where v is the shared vertex. For the task of discrimination, the subgraphs G_X are structurally symmetric, with symmetric vertices, $1_X, \cdots, n_X$, of which $1_C = 1_D = 1$ is shared, and symmetric edges, $i_C \to j_C$ if, and only if, $i_D \to j_D$. The labels on these corresponding edges may, however, be distinct. The vertices i_X with $i > 1$ are the microstates in which X is bound, while vertex 1 is the empty microstate in which no X is bound. All directed edges are assumed to be structurally reversible, so that, if $i_X \to j_X$, then $j_X \to i_X$. The graphs G_C, G_D, and G are therefore all strongly connected.

Let $G = G_C \oplus_v G_D$ be any butterfly graph. Even if G_C and G_D are not structurally symmetric, as above, it follows readily

from Eq. (1) that

$$\rho_i(G_C \oplus_v G_D) = \begin{cases} \rho_i(G_C)\rho_v(G_D) & \text{if } i \in G_C \\ \rho_i(G_D)\rho_v(G_C) & \text{if } i \in G_D. \end{cases} \quad (3)$$

IV. THE ERROR FRACTION FOR THE HOPFIELD MECHANISM

The original Hopfield kinetic proofreading mechanism is described by the discriminatory butterfly graph $G = G_C \oplus_1 G_D$ in Fig. 1(a). The substrates C and D are treated as "slow" components and assumed to have constant concentration over the timescale of interest. These concentrations are absorbed into the "on-rates" k'_C, k'_D, l'_C, l'_D. The discrimination mechanism itself is assumed to have the "fast" components and to be at steady state. The rate W for exit from 3_X ($X = C, D$) corresponds to product generation and release of X, so that the overall system is open whenever $W > 0$, with C and D being transformed into correct and incorrect product, respectively.

In this mechanism, discrimination occurs twice, through binding and unbinding of X to form 2_X and to form 3_X. It is assumed that unbinding, rather than binding, causes discrimination, as is often the case in biology [14], so that $l'_C = l'_D$ and $k'_C = k'_D$. The correct substrate has a longer residence time, so that $k_C < k_D$, which reflects the free energy difference of $\Delta > 0$ between 2_C and 2_D [Fig. 1(b)]: if energy is measured in units of $k_B T$, where k_B is Boltzmann's constant and T is the absolute temperature, then $k_D = k_C e^{\Delta}$. There is assumed to be no difference in discrimination between 2_X and 3_X, so that $k_C/k_D = l_C/l_D = e^{-\Delta} < 1$.

Hopfield defines the steady-state error fraction, ε as the probability ratio of the incorrect to the correct exit microstate, which, using Eq. (2), is given by $\varepsilon = \rho_{3_D}(G)/\rho_{3_C}(G)$ (ε is the inverse of the accuracy μ in the Abstract; we will work with the former). Using Eqs. (1) and (3),

$$\varepsilon = \frac{[l'_D(k_D + m') + m'k'_D][(k_C + m')(W + l_C) + mk_C]}{[l'_C(k_C + m') + m'k'_C][(k_D + m')(W + l_D) + mk_D]}. \quad (4)$$

If the overall system remains closed, so that $W = 0$, while the mechanism operates at thermodynamic equilibrium, then it has the error fraction, $\varepsilon_0 = k_C/k_D = l_C/l_D = e^{-\Delta}$ (Supplemental Material [43]). If the overall system becomes open, so that $W > 0$, while the mechanism remains at equilibrium, then ε increases monotonically with increasing W (Supplemental Material [43]). If the mechanism itself operates away from equilibrium, then

$$\varepsilon > \varepsilon_0 \left(\frac{l_C + m + W}{l_D + m + W} \right) > \varepsilon_0^2 \quad (5)$$

for all positive values of the parameters (Supplemental Material [43]). Hopfield shows that ε approaches the minimal error, ε_0^2, as certain parametric quantities become small (Supplemental Material [43]) and suggests how this could be achieved in practice by expending energy to drive the transition from 2_X to 3_X through the label m'. This is kinetic proofreading.

There are two aspects of Hopfield's analysis which have not always been fully appreciated. First, increasing m' is not sufficient of itself for ε to approach ε_0^2. Indeed, it follows from Eq. (4) that, when $W = 0$, $\varepsilon \to \varepsilon_0$ as $m' \to \infty$. Too much energy expenditure can increase the error fraction, which behaves nonmonotonically with respect to m'. (Similar nonmonotonicity has been observed for kinetic proofreading with the T-cell receptor mechanism in Supplemental Material Fig. 1 [18].) The parameter m' must neither be too high nor too low for the error fraction to approach ε_0^2. Second, parameters other than m', m, and W must also take adequate values for the accuracy to approach this bound: the "on-rate" for $1 \to 2_X$ must be much larger than that for $1 \to 3_X$, so that $l'_D/k'_D = l'_C/k'_C \to 0$ (Supplemental Material [43]). The lower bound of ε_0^2 is only reached asymptotically as several parameters take limiting values.

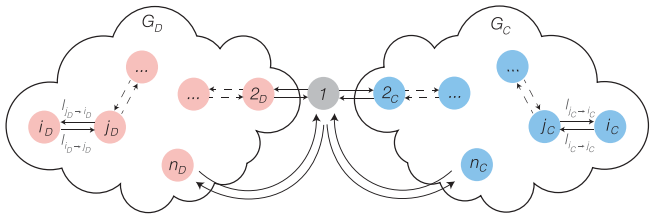

FIG. 2. Structure of dissociation-based mechanisms. Shown is a schematic of a labeled, directed "butterfly" graph illustrating the structure of any dissociation-based mechanism, which consists of the subgraph G_D for the incorrect substrate D and the subgraph G_C for the correct substrate C sharing the common vertex 1. G_C and G_D are assumed to be symmetric, but the internal transitions within them can be arbitrary, as suggested by the "clouds." n_X is taken to be the only exit microstate in which product is generated, so there is a return edge $n_X \to 1$. As in Fig. 1(a), cyan and magenta denote correct and incorrect substrate binding, respectively.

For more complex systems, the appropriate parameter regime for the minimal error is not readily found using Hopfield's approach. We therefore sought an alternative strategy. If we let $x = e^{\Delta} = \varepsilon_0^{-1}$ and substitute $k_D = xk_C$ and $l_D = xl_C$ into Eq. (4), we see that, if no other parameters change, the error fraction ε behaves like x^{-1} as x increases. We reasoned that to approach the minimal error of x^{-2}, the fold change in other parameter values should be some function of x. By retaining only the highest-order term in x as $x \to \infty$, the behavior of ε could be determined while bypassing the parametric complexity. Let $R(x) \sim Q(x)$ mean that $R(x)/Q(x) \to c$ as $x \to \infty$, where $0 < c < \infty$. It can be seen from Eq. (4) that if either $k'_D = k'_C \sim x$ or $l'_C = l'_D \sim x^{-1}$, while none of the remaining parameters depend on x, then $\varepsilon \sim x^{-2} = \varepsilon_0^2$. This scaling of the "on-rates" corresponds to what was required in the previous paragraph for Hopfield's limiting procedure. This suggests a strategy for exploring parameter space that can be extended to more complex systems. We exploit this below to examine the relation between energy, speed, and accuracy.

V. DISSOCIATION-BASED MECHANISMS

We introduce here a class of discrimination mechanisms for which such a relation can be determined. We consider a discriminatory butterfly graph of the form $G = G_C \oplus_1 G_D$ consisting of structurally symmetric subgraphs G_C and G_D of arbitrary complexity (Fig. 2). The vertex n_X is taken to be the only exit microstate in which product is generated, so that there is a return edge $n_X \to 1$. No further structural assumptions are

made but the product generation rate, W, makes an additive contribution to the label of the return edge $n_X \to 1$, as in Fig. 1(a).

Multiple internal microstates and transitions are allowed in G_X as well as multiple returns to the empty microstate, 1, although only a single one of these, through n_X, also generates product. As in Hopfield's original scheme, we think of the mechanism as coupled to sources and sinks of energy, which may alter the edge labels. In Hopfield's scheme, the labels on edges which do not go to the reference microstate 1 were assumed to be the same between C and D [Fig. 1(a)]. In other words, there was no "internal discrimination" between correct and incorrect substrates. Here, we allow internal discrimination between C and D: when $j \neq 1$, the label on $i_C \to j_C$ may be different from that on $i_D \to j_D$.

Graphs of this form been widely employed in the literature. In addition to the original Hopfield mechanism [Fig. 1(a)], they include the "delayed" mechanism [10], the multistep mechanism [12,13,44], the T-cell receptor mechanism [14,18], and generalized proofreading mechanisms [15–17].

We follow Hopfield in using the steady-state error fraction and work from now on with probabilities. Let p^* be the vector of steady state probabilities. The discrimination error fraction, ε, is the steady-state probability ratio of the incorrect exit microstate, n_D, to the correct exit microstate, n_C,

$$\varepsilon = \frac{p^*_{n_D}}{p^*_{n_C}}. \tag{6}$$

We will analyze the behavior of G under the assumption that some of the labels are functionally dependent on the nondimensional variable $x \in \mathbb{R}$. A function $R(x)$ is said to be allowable if it is positive, $R(x) > 0$ for $x > 0$, and has a degree, $\deg(R)$, given by $R(x) \sim x^{\deg(R)}$ as $x \to \infty$. This is well defined because $x^a \sim x^b$ if, and only if, $a = b$. The degree determines the asymptotics of allowable functions: $R \sim Q$ if, and only if, $\deg(R) = \deg(Q)$. Note that $\deg(R) = 0$ if, and only if, $R(x) \to c$ as $x \to \infty$, where $c > 0$, which is the case if R does not depend on x.

The labels in the graph G are assumed to be allowable functions of x. (The product generation rate W couples the mechanism to the environment and is assumed not to depend on x.) If R and Q are allowable functions, then so are R^{-1}, RQ, and $R + Q$ and (Supplemental Material [43]):

$$\begin{aligned} \deg(R^{-1}) &= -\deg(R), \\ \deg(RQ) &= \deg(R) + \deg(Q), \\ \deg(R+Q) &= \max(\deg(R), \deg(Q)). \end{aligned} \tag{7}$$

Accordingly, any rational function of the labels with only positive terms, such as p^*, which acquires this structure through Eqs. (2) and (1), or ε, which acquires it through Eq. (6), becomes in turn an allowable function of x.

We define a dissociation-based mechanism to be a general discrimination mechanism for which, for the edges between the exit microstates and 1,

$$\begin{aligned} \deg(\ell_{1\to n_D}) &= \deg(\ell_{1\to n_C}), \\ \deg(\ell_{n_D\to 1}) &= \deg(\ell_{n_C\to 1}) + 1. \end{aligned} \tag{8}$$

Here, we use $\ell_{i\to j}$ to denote the label on the edge $i \to j$. Equation (8) is analogous to the assumption $l'_C = l'_D$ and $xl_C = l_D$ for the Hopfield mechanism. Unlike the Hopfield mechanism, we do not restrict what happens at nonexit microstates.

With such general assumptions on the labels, a dissociation-based mechanism may not reach thermodynamic equilibrium. However, if it can, with $W > 0$, so that the overall system remains open, then Eq. (8) ensures that the equilibrium error fraction, ε_{eq}, has a simple form. Since detailed balance requires that each pair of edges is independently at steady state [36], the exit states, n_X, satisfy $\ell_{n_X\to 1} p^*_{n_X} = \ell_{1\to n_X} p^*_1$, so that

$$\varepsilon_{\rm eq} = \frac{p^*_{n_D}}{p^*_{n_C}} = \left(\frac{\ell_{1\to n_D}}{\ell_{1\to n_C}}\right)\left(\frac{\ell_{n_C\to 1}}{\ell_{n_D\to 1}}\right). \tag{9}$$

Applying Eq. (8) and using Eq. (6), we see that, if equilibrium is reached, the resulting error fraction, $\varepsilon_{\rm eq}$, satisfies

$$\varepsilon_{\rm eq} \sim x^{-1}. \tag{10}$$

VI. THE ASYMPTOTIC RELATION

We now define the measures of speed and energy expenditure in terms of which our main result will be stated. A reasonable interpretation for the speed of the mechanism, σ, is the steady-state flux of correct product [45],

$$\sigma = W p^*_{n_C}. \tag{11}$$

As for energy expenditure, this is determined at steady state by the rate of entropy production. Schnakenberg put forward a definition of this [42] that has been widely used [2,7]: for a pair of reversible edges, $i \rightleftarrows j$, the steady-state entropy production rate, $P(i \rightleftarrows j)$, is the product of the net flux, $J(i \rightleftarrows j) = \ell_{j\to i} p^*_j - \ell_{i\to j} p^*_i$, and the thermodynamic force, $A(i \rightleftarrows j) = \ln(\ell_{j\to i} p^*_j / \ell_{i\to j} p^*_i)$:

$$P(i \rightleftarrows j) = J(i \rightleftarrows j) A(i \rightleftarrows j). \tag{12}$$

Here, we omitted Boltzmann's constant k_B for convenience, so that P has units of (time)$^{-1}$. If T is the absolute temperature, then $k_B T P(i \rightleftarrows j)$ is the power irreversibly expended through $i \rightleftarrows j$. The total entropy production rate of the system is then given by $P = \sum_{i\rightleftarrows j} P(i \rightleftarrows j)$. Note that $P(i \rightleftarrows j) \geqslant 0$ (and so also $P \geqslant 0$) with equality at thermodynamic equilibrium when detailed balance implies that $J(i \rightleftarrows j) = 0$. Positive entropy production, with $P > 0$, signifies energy expenditure away from thermodynamic equilibrium.

Both σ and P are functions of x and σ is evidently allowable. However, $A(i \rightleftarrows j)$ is not a rational function with positive terms and $\ln(x) \not\sim x^\alpha$ for any α, so $P(i \rightleftarrows j)$ and P are not allowable functions. Nevertheless, the asymptotic behavior of P can be estimated. Some further notation is helpful to do this. If $R(x)$ and $Q(x)$ are functions which are not necessarily allowable, then $R \prec Q$ means that $R/Q \to 0$ as $x \to \infty$. This relation is transitive, so that, if $S \prec R$ and $R \prec Q$, then $S \prec Q$. If both functions are allowable, then $R \prec Q$, if, and only if, $\deg(R) < \deg(Q)$. We will say that $R \precsim Q$ if $R/Q \to c$, where $0 \leqslant c < \infty$, and corresponding remarks about transitivity and allowable degrees hold for this relation. Note that $\prec$ and $\precsim$ dominate over $\sim$ when forming

products, so, for instance,

$$\text{if } T \precsim S \text{ and } R \sim Q \text{ then } RT \precsim SQ, \tag{13}$$

which we will make use of below.

Each summand $P(i \rightleftarrows j)$ has the form $(R - Q)\ln(R/Q)$, where R and Q are allowable. Let $\alpha = \deg(R)$, $\beta = \deg(Q)$ and $c_1 = \lim R/x^\alpha$ and $c_2 = \lim Q/x^\beta$ as $x \to \infty$. By definition, $c_1, c_2 > 0$. Note that, if S is allowable, then (Supplemental Material [43])

$$\ln(S) \sim \begin{cases} \ln(x) & \text{if } \deg(S) > 0 \\ \ln(x^{-1}) & \text{if } \deg(S) < 0. \end{cases} \tag{14}$$

The asymptotic behavior of $P(i \rightleftarrows j)$ then falls into the following three cases (Supplemental Material [43]), as specified on the right:

$$\begin{array}{lccc} \textbf{case 1:} & \alpha \neq \beta & \sim x^{\max(\alpha,\beta)}\ln(x), \\ \textbf{case 2:} & \alpha = \beta, c_1 \neq c_2 & \sim x^\alpha, \\ \textbf{case 3:} & \alpha = \beta, c_1 = c_2 & \prec x^\alpha. \end{array} \tag{15}$$

The third case is awkward because the leading-order asymptotics are lost, which leads to the $\prec$ relation instead of $\sim$. However, c_1 and c_2 are rational expressions in the parameters, which do not involve x, and the equation $c_1 = c_2$ defines a hypersurface in the space of those parameters. The reversible edges which fall into case 3 therefore determine a set of measure zero in the space of parameters. Provided this set is avoided, the asymptotic behavior of the summands in P fall into the first two cases and can be controlled. In particular, suppose that the total entropy production rate P is written as $P = \sum_u P_u$, where P_u is a term coming from a pair of reversible edges $i \rightleftarrows j$, as in Eq. (12). In Appendix A, we show that, if P_k is any summand in case 1 of Eq. (15), then, outside the measure-zero set defined by case 3, $P_k \precsim P$.

Let us now assume, for any dissociation-based mechanism as defined previously, that

$$\varepsilon(x) \prec x^{-1}. \tag{16}$$

This forces the error fraction to be asymptotically better than if the system were able to reach equilibrium [Eq. (10)] and thereby ensures that energy expenditure is contributing to an improvement in accuracy. Consider any general discrimination mechanism which is dissociation-based, as described in Eq. (8). If its error fraction obeys Eq. (16) then, outside the measure-zero set in parameter space defined by case 3 of Eq. (15), we show in Appendix B that the mechanism satisfies the asymptotic relation,

$$\sigma \ln(\varepsilon^{-1}) \precsim P. \tag{17}$$

The exact asymptotics of $\sigma \ln(\varepsilon^{-1})/P$ are difficult to estimate for a general dissociation-based mechanism with allowable labels because each pair of reversible edges must be examined. However, for the Hopfield mechanism [Fig. 1(a)], under the conditions described above for which $\varepsilon \sim x^{-2}$, we find (Supplemental Material [43])

$$\lim_{x\to\infty} \frac{\sigma \ln(\varepsilon^{-1})}{P} = \frac{2W}{l_c + W} \tag{18}$$

outside the parametric set of measure-zero noted above.

VII. A NONDISSOCIATION-BASED MECHANISM

The requirements in Eq. (8) for being dissociation-based are necessary for the validity of Eq. (17). In the Supplemental Material [43], we consider a discrimination mechanism with a structure identical to that of the Hopfield mechanism [Fig. 1(a)] but with labels that do not follow Eq. (8) (Supplemental Material Fig. 3 [43]). If the mechanism reaches thermodynamic equilibrium, then it follows from Eq. (9) that its equilibrium error fraction satisfies $\varepsilon_{\text{eq}} \sim x^{-1}$. However, with a particular choice of allowable functions for the labels, for which the mechanism is no longer at equilibrium, its error fraction improves asymptotically, with $\varepsilon \sim x^{-3/2}$, while its speed remains constant, $\sigma \sim 1$, and its entropy production is either constant or vanishes, $P \precsim 1$, outside a set of measure zero. This evidently does not obey Eq. (17) and shows the existence of a different asymptotic interplay between energy, speed and accuracy.

VIII. NUMERICAL CALCULATIONS OUTSIDE THE ASYMPTOTIC REGIME

To examine further the energy-speed-accuracy relation found by the asymptotic analysis above, we used more restrictive assumptions on the allowable labels to facilitate numerical exploration. We considered discrimination-based mechanisms in which the x-dependency was similar to Hopfield's original analysis. For any return edge to 1 from a nonexit microstate, we assumed that

$$\ell_{i_D\to 1} = \ell_{i_C\to 1} x \ (i \neq n), \tag{19}$$

with an additive contribution of W in the exit microstate ($i = n$), $\ell_{n_D\to 1} = ax + W$, $\ell_{n_C\to 1} = a + W$ with $a \in \mathbb{R}_{>0}$. As for the other edges, we assumed no internal discrimination, so that the labels were the same for C and D,

$$\ell_{i_D\to j_D} = \ell_{i_C\to j_C} \ (j \neq 1), \tag{20}$$

with no x-dependency. By Eq. (9), the equilibrium error function when the system is closed ($W = 0$) satisfies $\varepsilon_0 = x^{-1}$. We set $x = e^{20}$, sampled the values $\ln(\ell_{i_C\to j_C})$, $\ln(a)$, and $\ln(W)$ uniformly in $[-100, 100]$, and determined $\ell_{i_D\to j_D}$ from Eqs. (19) and (20). We plotted P/σ against $\ln(\varepsilon_0/\varepsilon)$, when $\varepsilon < \varepsilon_0$, for the Hopfield mechanism [Fig. 3(a)], the T-cell receptor mechanism (Supplemental Material Fig. 1) and for a mechanism different from both of these (Supplemental Material Fig. 2). In each case, the resulting region was confined to the left of a vertical line [Fig. 3(a), black dashed line] and above the diagonal [Fig. 3(a), red dashed line]. For the Hopfield mechanism, the vertical bound comes from Eq. (5) and similar bounds on ε exist for the other mechanisms (not shown). The diagonal bound, however, is unexpected and implies the bound

$$\sigma \ln(\varepsilon_0/\varepsilon) < P \quad (\text{for } \varepsilon < \varepsilon_0) \tag{21}$$

for finite parameter values. It is possible that Eq. (21) holds for any discrimination-based mechanism whose edge labels satisfy Eqs. (19) and (20).

The calculations leading to Eq. (21) assumed no internal discrimination between correct and incorrect substrate, as

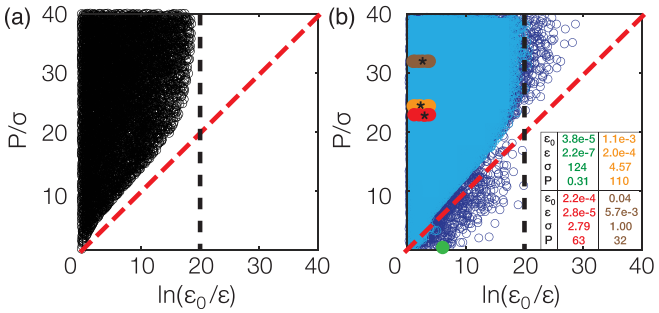

FIG. 3. Numerics for the Hopfield mechanism. (a) Plot of P/σ against $\ln(\varepsilon_0/\varepsilon)$ for the Hopfield mechanism [Fig. 1(a)] for approximately 10^5 points. The sampling and the dashed lines are described in the text. (b) Similar plot to (a) for the Hopfield mechanism with internal discrimination between correct and incorrect substrates, as described in the text, with the light blue points having a lower asymmetry range ($A = 1$) and the dark blue points having a higher range ($A = 5$). The colored overlays represent values from experimental data for ribosomes (orange, red and brown regions) and DNA polymerase (green point), with the former being samples of values estimated for a parameter for which no experimental data exists. Only those samples for which $\varepsilon > \varepsilon_0$ are shown and the asterisks, *, give the averages of the plotted values. The inset gives the plotted averages (for the ribosome variants) and values (for DNAP) of error fractions, ε and ε_0 (which are nondimensional), and speed, σ and entropy production rate, P (in units of s^{-1}). The data from which these values were calculated are shown in Supplemental Material Table 1. See Ref. [46] and the caption of Supplemental Material Table 1 for more details.

specified in Eq. (20). We were interested to find that experimental data for ribosomes and DNA polymerase, based on the original Hopfield mechanism, showed substantial internal discrimination, extending even to the product generation rate W [19]. To examine the impact of this, we proceeded as follows. For any return edge to 1 from a nonexit microstate, we introduced an asymmetry between C and D so that

$$\ell_{i_D\to 1} = \alpha_{i1}\ell_{i_C\to 1}x \ (i \neq n). \tag{22}$$

For the exit state ($i = n$), the product generation rate makes an additive contribution, W_X, which now depends on the substrate X, so that $\ell_{n_C\to 1} = a + W_C$ and $\ell_{n_D\to 1} = \alpha_{n1}ax + W_D$, where $a \in \mathbb{R}_{>0}$ and $W_D = \alpha_W W_C$. For the other edges, we similarly introduced an asymmetry

$$\ell_{i_D\to j_D} = \alpha_{ij}\ell_{i_C\to j_C} \ (j \neq 1). \tag{23}$$

The multiplicative factors α_{ij} and α_W carry the asymmetry between C and D in internal discrimination.

In view of the asymmetry in product generation rates, it is natural to redefine the error fraction as

$$\varepsilon = \frac{W_D p^*_{n_D}}{W_C p^*_{n_C}}.$$

Using Eq. (9), the equilibrium error fraction when the system is closed ($W = 0$) is given by $\varepsilon_0 = \ell_{1\to n_D}a/(\ell_{1\to n_C}\alpha_{n1}a)$.

We chose the asymmetry factors by sampling $\ln(\alpha_{ij})$ and $\ln(\alpha_W)$ uniformly in the range $[-A, A]$, for $A = 1$ and $A = 5$, and chose the other parameters as described previously for Fig. 3(a). Figure 3(b) shows that both the vertical bound and the diagonal bound in Fig. 3(a) are broken, with the extent of the breach increasing with increase in the asymmetry range from $A = 1$ [Fig. 3(b), light blue points] to $A = 5$ [Fig. 3(b), dark blue points]. Similar results were found for the other mechanisms that we numerically calculated [Supplemental Material Figs. 1(c) and 2(c)]. We see that the absence of internal discrimination is essential for the vertical and diagonal bounds shown in Fig. 3(a) and Supplemental Material Figs. 1(b) and 2(b).

Banerjee *et al.* have provided parameter values for the Hopfield mechanism based on experimental data for discrimination in mRNA translation by the *Escherichia coli* ribosome, including also an error-prone and a hyperaccurate mutant, and in DNA replication by the bacteriophage T7 DNA polymerase (DNAP) [19]. We used these parameter values to calculate entropy production, speed and accuracy as defined here and overlaid the resulting $\ln(\varepsilon_0/\varepsilon)$, P/σ points on the previous numerical calculation [Fig. 3(b)] [46].

The data show a striking difference between mRNA translation and DNA replication [Fig. 3(b)]. All three ribosome variants (orange, wild type; brown, error-prone; red, hyperaccurate) have much higher P/σ values than DNAP (green), with the former lying comfortably above the diagonal bound given by Eq. (21) and the latter lying well below. Nevertheless, all systems exhibit substantial internal discrimination (Supplemental Material Table 1). As the inset in Fig. 3(b) shows, the separation between translation and replication arises from a decrease of two orders of magnitude in entropy production rate and an increase of two orders of magnitude in speed. Furthermore, DNAP not only shows the smallest error fraction, ε, by three orders of magnitude, but also the greatest fold change over the equilibrium error fraction, $\varepsilon_0/\varepsilon$. In contrast, the ribosome variants, while showing the expected differences in error fraction, have lower fold changes over their equilibrium error fractions. Evolution seems to have tuned the energy dissipation, speed, and accuracy of the replication machinery to a much greater degree than the translation machinery.

IX. DISCUSSION

One of the challenges in dealing with nonequilibrium systems in general has been the algebraic complexity, as epitomized by the enumeration of spanning trees in the MTT, Eq. (1). For a complicated graph, the combinatorial explosion in enumerating spanning trees can be super-exponential in the size of the graph [8]. This difficulty may have been apparent to earlier workers like Hill [41] and Schnakenberg [42] and may have discouraged a more analytical approach. The combinatorial complexity has largely been avoided by focusing on simple or highly structured examples and by astute use of approximation.

In this paper, we have developed a way to address this complexity that is inspired by Hopfield's analysis of kinetic proofreading. Here, the minimum error fraction can only be reached asymptotically [Eq. (5)] and only when multiple labels change their values consistently. This has suggested a method of exploring parameter space by treating the labels as allowable functions of a scaling variable x. In this way, a system of arbitrary structure can be analyzed away from equilibrium,

with relaxed assumptions on how energy is being deployed, while rising above the combinatorial explosion.

Perhaps the most interesting conclusion from this analysis is the emergence of the quantity $\sigma \ln(\mu)/P$. Our main result, as expressed in Eq. (17), says that this quantity is asymptotically finite, for any graph obeying the dissociation-based condition on exit edges [Eq. (8)] and for any scheme of allowable scaling through which energy increases ($\deg > 0$) or decreases ($\deg < 0$) the rates, provided that the accuracy improves over equilibrium [Eq. (16)].

The advantage of the asymptotic analysis undertaken here is that it reveals a universal behavior in $\sigma \ln(\mu)/P$ that transcends network structure and parametric complexity. Interestingly, our numerical calculations suggest that universality may still be found for finite parameter values, in the form of the bound in Eq. (21), as shown in Fig. 3 and Supplemental Material Figs. 1 and 2. However, this bound depends crucially on the absence of internal discrimination between correct and incorrect substrates, in contrast to the asymptotic behavior in Eq. (17), for which internal discrimination is allowed. Experimental data shows that evolution has discriminated internally to a substantial extent but with very different effects on this bound. All *E. coli* ribosome variants for which we have data comfortably obey the bound, while the T7 DNA polymerase breaks it. This reflects a striking reduction in P/σ for the latter, with far less difference between the ribosomes and the DNA polymerase in the fold change over their equilibrium error fractions [Fig. 3(b)]. It would be interesting to know if these same comparative relationships are maintained for other ribosomes and polymerases. While recent work has shown that local trade-offs between speed and accuracy can differ markedly between different parametric regions [19], the quantities introduced here may be helpful for more global comparisons between discriminatory mechanisms.

As noted in the Introduction, the previous work of Refs. [17,25,35] shows formal similarities to the results presented here and it may be helpful to clarify these connections. In Ref. [35], England and colleagues determine the minimal energy dissipation cost for a general finite-state Markov process to maintain an arbitrary nonequilibrium steady state. While their setting is similar to our graph-theoretic approach, they assume that energy is introduced through additional control transitions and their analysis of maintenance does not involve notions of speed or accuracy as used to analyze discrimination. In Ref. [25], Tu and colleagues study the costs of adaptation and derive an approximate relationship between the rate of energy dissipation and the speed and accuracy of adaptation [their Eqs. (5) and (S18)]. Their formulas resemble our Eq. (17). They infer their results from a continuum model of a three-state negative-feedback system, using the Fokker-Planck equation for the time evolution of the probability density and undertake the approximation by steepest descent on the adaptation error. The similarity in results despite the very different methods supports the analogy that has been drawn previously between adaptation and discrimination [3]. However, the work of Ref. [25] is limited to a three-state system, while our results apply to systems of arbitrary complexity. In Ref. [17], Sartori and Pigolotti determine the thermodynamic cost of copying a biopolymer. The copying process includes a discrimination mechanism that chooses between right and wrong monomers for incorporation in the polymer. They adopt a general finite-state Markov process, as in Ref. [35], and rely on the second law of thermodynamics to derive a bound for the total entropy production per wrongly incorporated monomer [their Eq. (3)]. They identify three operating regimes, of which the third, called "error correction," resembles that studied here and yields a formula which is similar to our Eq. (17). Their formula expresses a finite bound and involves only quantities related to discrimination of the wrong monomer, while our formula is valid asymptotically and compares right and wrong discriminations. The two studies can be seen as offering complementary approaches to the problem of algebraic complexity away from thermodynamic equilibrium: Sartori and Pigolotti appeal to the second law of thermodynamics while we exploit leading-order asymptotics as $x \to \infty$.

In summary, our work offers methods to rise above the algebraic complexity characteristic of nonequilibrium Markov processes and suggests that the quantity $\sigma \ln(\mu)/P$ may be significant for a broader context of cellular information processing that includes discrimination, adaptation, and other processes required for life. Because of their generality, the methods used here may be particularly useful for developing such a broader perspective.

ACKNOWLEDGMENTS

F.W. was supported by the National Science Foundation (NSF) Graduate Research Fellowship under Grant No. DGE1144152. A.A. was supported by the Alfred P. Sloan Foundation. J.G. was supported by NSF Grant No. 1462629. We thank P.-Y. Ho and J. Horowitz for discussions.

APPENDIX A: PROOF OF $P_k \precsim P$

Suppose that $P_k \sim x^{\alpha_k} \ln(x)$. If P_i is also in case 1 and $P_i \sim x^{\alpha_i} \ln(x)$, then $P_i/P_k \to c$, where $c = 0, 1, \infty$, depending on the relative values of α_i and α_k. Similarly, if P_j is in case 2 and $P_j \sim x^{\alpha_j}$, then $P_j/P_k \to c$, where $c = 0, \infty$, depending on the relative values of α_j and α_k. By assumption, there are no other cases to consider (if P_h were in case 3, we could not estimate $\lim_{x\to\infty} P_h/P_k$). Since P_k is one of the summands in P, it follows that $P/P_k \to c$, where $1 \leqslant c \leqslant \infty$. Equivalently, $P_k/P \to c^{-1}$, where $0 \leqslant c^{-1} \leqslant 1$. In particular, $P_k \precsim P$, as required.

APPENDIX B: PROOF OF THE ASYMPTOTIC RELATION

Suppose first that $1 \rightleftarrows n_C$ falls into case 1 in Eq. (15). Let $\alpha = \deg(\ell_{n_C\to 1} p^*_{n_C})$ and $\beta = \deg(\ell_{1\to n_C} p^*_1)$, so that $\alpha \neq \beta$. Then, $x^\alpha \ln(x) \precsim x^{\max(\alpha,\beta)} \ln(x) \sim P(1 \rightleftarrows n_C)$. Since the product generation rate, W, appears additively, $\ell_{n_C\to 1} = W + U(x)$, for some allowable function U. It follows from Eq. (7) that $\alpha = \deg(\ell_{n_C\to 1}) + \deg(p^*_{n_C}) = \max(0, \deg(U)) + \deg(p^*_{n_C}) \geqslant \deg(W p^*_{n_C}) = \deg(\sigma)$. Hence, $\sigma \precsim x^\alpha$. Furthermore, since Eq. (16) tells us that $\deg(\varepsilon) < -1$, it follows from Eq. (14) that $\ln(\varepsilon^{-1}) \sim \ln(x)$. Using Eq. (13),

we deduce that

$$\sigma \ln(\varepsilon^{-1}) \precsim P(1 \rightleftarrows n_C).$$

If $1 \rightleftarrows n_C$ does not fall into case 1 in Eq. (15), then $\alpha = \beta$. Let us then consider $1 \rightleftarrows n_D$. According to Eqs. (6) and (16), $\deg(p^*_{n_D}) < \deg(p^*_{n_C}) - 1$. Using Eq. (7) to combine this with Eq. (8), we see that $\deg(\ell_{n_D \to 1} p^*_{n_D}) < \deg(\ell_{n_C \to 1} p^*_{n_C}) = \alpha = \beta = \deg(\ell_{1 \to n_C} p^*_1)$. But now, by Eqs. (8) and (7),

$$\deg(\ell_{1 \to n_C} p^*_1) = \deg(\ell_{1 \to n_D} p^*_1). \tag{B1}$$

It follows that

$$\deg(\ell_{n_D \to 1} p^*_{n_D}) < \deg(\ell_{1 \to n_D} p^*_1), \tag{B2}$$

so that $1 \rightleftarrows n_D$ falls into case 1 even though $1 \rightleftarrows n_C$ does not. Therefore, by Eq. (15), $P(1 \rightleftarrows n_D) \sim x^\gamma \ln(x)$, in which, because of Eq. (B2), $\gamma = \deg(\ell_{1 \to n_D} p^*_1)$. But according to Eq. (B1), $\gamma = \deg(\ell_{1 \to n_C} p^*_1) = \beta = \alpha$. Hence, by the same argument as above for $1 \rightleftarrows n_C$, we deduce that

$$\sigma \ln(\varepsilon^{-1}) \precsim P(1 \rightleftarrows n_D).$$

We can now appeal to the result in Appendix A to complete the proof.

[1] H. C. Berg and E. M. Purcell, Physics of chemoreception, Biophys. J. **20**, 193 (1977).

[2] P. Mehta and D. J. Schwab, Energetic costs of cellular computation, Proc. Natl. Acad. Sci. USA **109**, 17978 (2012).

[3] D. Hartich, A. C. Barato, and U. Seifert, Nonequilibrium sensing and its analogy to kinetic proofreading, New J. Phys. **17**, 055026 (2015).

[4] P. R. ten Wolde, N. B. Becker, T. E. Ouldridge, and A. Mugler, Fundamental limits to cellular sensing, J. Stat. Phys. **163**, 1395 (2016).

[5] V. Singh and I. Nemenman, Simple biochemical networks allow accurate sensing of multiple ligands with a single receptor, PLoS Comput. Biol. **13**, e1005490 (2017).

[6] H. Qian and J. A. Cooper, Temporal cooperativity and sensitivity amplification in biological signal transduction, Biochemistry **47**, 2211 (2008).

[7] Y. Tu, The nonequilibrium mechanism for ultrasensitivity in a biological switch: sensing by Maxwell's demons, Proc. Natl. Acad. Sci. USA **105**, 11737 (2008).

[8] J. Estrada, F. Wong, A. DePace, and J. Gunawardena, Information integration and energy expenditure in gene regulation, Cell **166**, 234 (2016).

[9] J. J. Hopfield, Kinetic proofreading: a new mechanism for reducing errors in biosynthetic processes requiring high specificity, Proc. Natl. Acad. Sci. USA **71**, 4135 (1974).

[10] J. Ninio, Kinetic amplification of enzyme discrimination, Biochemie **57**, 587 (1975).

[11] C. H. Bennett, Dissipation error tradeoff in proofreading, BioSystems **11**, 85 (1979).

[12] C. Blomberg and M. Ehrenberg, Energy considerations for kinetic proofreading in biosynthesis, J. Theor. Biol. **88**, 631 (1981).

[13] M. A. Savageau and D. S. Lapointe, Optimization of kinetic proofreading: A general method for derivation of the constraint relations and an exploration of a specific case, J. Theor. Biol. **93**, 157 (1981).

[14] T. W. McKeithan, Kinetic proofreading in T-cell receptor signal transduction, Proc. Natl. Acad. Sci. USA **92**, 5042 (1995).

[15] A. Murugan, D. A. Huse, and S. Leibler, Speed, dissipation, and error in kinetic proofreading, Proc. Natl. Acad. Sci. USA **109**, 12034 (2012).

[16] A. Murugan, D. A. Huse, and S. Leibler, Discriminatory Proofreading Regimes in Nonequilibrium Systems, Phys. Rev. X **4**, 021016 (2014).

[17] P. Sartori and S. Pigolotti, Thermodynamics of Error Correction, Phys. Rev. X **5**, 041039 (2015).

[18] W. Cui and P. Mehta, Optimality in kinetic proofreading and early T-cell recognition: Revisiting the speed, energy, accuracy trade-off, arXiv:1703.03398.

[19] K. Banerjee, A. B. Kolomeisky, and O. A. Igoshin, Elucidating interplay of speed and accuracy in biological error correction, Proc. Natl. Acad. Sci. USA **114**, 5183 (2017).

[20] K. Banerjee, A. B. Kolomeisky, and O. A. Igoshin, Accuracy of substrate selection by enzymes is controlled by kinetic discrimination, J. Phys. Chem. Lett. **8**, 1552 (2017).

[21] R. Rao and L. Peliti, Thermodynamics of accuracy in kinetic proofreading: Dissipation and efficiency trade-offs, J. Stat. Mech. Theor. Exp. (2015) P06001.

[22] M. Ehrenberg and C. Blomberg, Thermodynamic constraints on kinetic proofreading in biosynthetic pathways, Biophys. J. **31**, 333 (1980).

[23] R. R. Freter and M. A. Savageau, Proofreading systems of multiple stages for improved accuracy of biological discrimination, J. Theor. Biol. **85**, 99 (1980).

[24] P. Sartori and S. Pigolotti, Kinetic Versus Energetic Discrimination in Biological Copying, Phys. Rev. Lett. **110**, 188101 (2013).

[25] G. Lan, P. Sartori, S. Neumann, V. Sourjik, and Y. Tu, The energy-speed-accuracy trade-off in sensory adaptation, Nat. Phys. **8**, 422 (2012).

[26] T. E. Holy and S. Leibler, Dynamic instability of microtubules as an efficient way to search in space, Proc. Natl. Acad. Sci. USA **91**, 5682 (1994).

[27] A. H. Lang, C. K. Fisher, T. Mora, and P. Mehta, Thermodynamics of Statistical Inference by Cells, Phys. Rev. Lett. **113**, 148103 (2014).

[28] P. Sartori, L. Granger, C. F. Lee, and J. M. Horowitz, Thermodynamic costs of information processing in sensory adaptation, PLoS Comp. Biol. **10**, e1003974 (2014).

[29] J. M. R. Parrondo, J. M. Horowitz, and T. Sagawa, Thermodynamics of information, Nat. Phys. **11**, 131 (2015).

[30] S. Still, D. A. Sivak, A. J. Bell, and G. E. Crooks, Thermodynamics of Prediction, Phys. Rev. Lett. **109**, 120604 (2012).

[31] J. Das, Limiting energy dissipation induces glassy kinetics in single-cell high-precision responses, Biophys. J. **110**, 1180 (2016).

[32] T. Ahsendorf, F. Wong, R. Eils, and J. Gunawardena, A framework for modeling gene regulation which accommodates non-equilibrium mechanisms, BMC Biol. **12**, 102 (2014).

[33] H. Qian, Reducing intrinsic biochemical noise in cells and its thermodynamic limit, J. Mol. Biol. **362**, 387 (2006).

[34] M. Nguyen and S. Vaikuntanathan, Design principles for nonequilibrium self-assembly, Proc. Natl. Acad. Sci. USA **113**, 14231 (2016).

[35] J. Horowitz, K. Zhou, and J. England, Minimum energetic cost to maintain a target nonequilibrium state, Phys. Rev. E **95**, 042102 (2017).

[36] J. Gunawardena, A linear framework for time-scale separation in nonlinear biochemical systems, PLoS ONE **7**, e36321 (2012).

[37] I. Mirzaev and J. Gunawardena, Laplacian dynamics on general graphs, Bull. Math. Biol. **75**, 2118 (2013).

[38] J. Gunawardena, Time-scale separation: Michaelis and Menten's old idea, still bearing fruit, FEBS J. **281**, 473 (2014).

[39] M. Thomson and J. Gunawardena, Unlimited multistability in multisite phosphorylation systems, Nature **460**, 274 (2009).

[40] T. Dasgupta, D. H. Croll, J. A. Owen, M. G. Vander Heiden, J. W. Locasale, U. Alon, L. C. Cantley, and J. Gunawardena, A fundamental trade off in covalent switching and its circumvention by enzyme bifunctionality in glucose homeostasis, J. Biol. Chem. **289**, 13010 (2014).

[41] T. L. Hill, Studies in irreversible thermodynamics IV. Diagrammatic representation of steady state fluxes for unimolecular systems, J. Theor. Biol. **10**, 442 (1966).

[42] J. Schnakenberg, Network theory of microscopic and macroscopic behavior of master equation systems, Rev. Mod. Phys. **48**, 571 (1976).

[43] See Supplemental Material at http://link.aps.org/supplemental/10.1103/PhysRevE.98.012420 for proofs of results in the main text, three supplemental figures and one supplemental table.

[44] M. Johansson, M. Lovmar, and M. Ehrenberg, Rate and accuracy of bacterial protein synthesis revisited, Curr. Opin. Microbiol. **11**, 141 (2008).

[45] T. L. Hill, *Free Energy Transduction and Biochemical Cycle Kinetics* (Dover Publications, New York, 2004).

[46] We note that Banerjee *et al.* imposed one additional constraint on their numerical values, following Ref. [3], by assuming that the correct and incorrect substrates used the same external chemical potential to break thermodynamic equilibrium; see Eq. (2) in Ref. [19]. While this is reasonable, we have followed Hopfield here and not made that assumption in our analysis and calculations. We also had to estimate two parameter values for the ribosome variants in Fig. 3(b), for which experimental data were not available, and did so by random sampling, as explained in Table 1 of the Supplemental Material [43].

Supplementary Material: An energy-speed-accuracy relation in complex networks for biological discrimination

Felix Wong,[1,2] Ariel Amir,[1] and Jeremy Gunawardena[2,*]
[1]*School of Engineering and Applied Sciences, Harvard University, Cambridge, MA 02138, USA*
[2]*Department of Systems Biology, Harvard Medical School, Boston, MA 02115, USA*

We provide proofs here of the mathematical assertions made in the main text.

I. EQUILIBRIUM ERROR FRACTION FOR THE HOPFIELD MECHANISM

The error fraction, ε, for the Hopfield mechanism is given in equation (4) of the main text, and is repeated here for convenience,

$$\varepsilon = \frac{[l'_D(k_D+m')+m'k'_D][(k_C+m')(W+l_C)+mk_C]}{[l'_C(k_C+m')+m'k'_C][(k_D+m')(W+l_D)+mk_D]}\,. \tag{1}$$

The background assumptions, as mentioned in the main text, are $k'_C = k'_D$, $l'_C = l'_D$ and $k_C/k_D < 1$.

If the mechanism is at thermodynamic equilibrium, then detailed balance must be satisfied. The equivalent cycle condition [1] applied to the two cycles in Fig. 1(a) of the main text yields

$$\frac{m'}{m} = \frac{l'_C k_C}{l_C k'_C} = \frac{l'_D k_D}{l_D k'_D}\,. \tag{2}$$

Note that W does not appear in equation (2) since, although the mechanism itself is at thermodynamic equilibrium, the system remains open, with substrate being converted to product. Denote by ε_{eq} the value of ε under the equilibrium constraint in equation (2). Using equation (2), define α, β so that

$$\alpha = \frac{l_C}{l'_C} = \frac{mk_C}{m'k'_C} \text{ and } \beta = \frac{l_D}{l'_D} = \frac{mk_D}{m'k'_D}\,.$$

Using the background assumptions, define the quantity ε_0, given by

$$\varepsilon_0 = \frac{\alpha}{\beta} = \frac{l_C}{l_D} = \frac{k_C}{k_D}\,, \tag{3}$$

to which a physical interpretation will be given shortly. Substituting α and β into equation (1) and rewriting, we see that

$$\varepsilon_{eq} = \frac{W.A+\alpha}{W.B+\beta}\,,$$

where

$$A = \frac{k_C+m'}{(k_C+m')l'_C+m'k'_C}\,,\quad B = \frac{k_D+m'}{(k_D+m')l'_D+m'k'_D}\,.$$

If $W = 0$, then by equation (3), $\varepsilon_{eq} = \varepsilon_0$, which shows that ε_0, as defined in equation (3), is the error fraction for the closed system at thermodynamic equilibrium as defined in the main text.

We now want to prove that ε_{eq} increases from ε_0 as W increases, for which it is sufficient to show that $d\varepsilon_{eq}/dW > 0$. For this,

$$\frac{d\varepsilon_{eq}}{dW} = \frac{A\beta - B\alpha}{(W.B+\beta)^2}\,,$$

so that $d\varepsilon_{eq}/dW > 0$ if, and only if, $A/B > \alpha/\beta$. We have

$$\frac{A}{B} = \left(\frac{k_C+m'}{k_D+m'}\right)\left(\frac{(k_D+m')l'_D+m'k'_D}{(k_C+m')l'_C+m'k'_C}\right)\,. \tag{4}$$

The following result is straightforward.

Lemma. *Consider the rational function $r(x) = (a+x)/(b+x)$, where $a, b > 0$. If $a/b > 1$, then $r(x)$ decreases strictly monotonically from $r(0) = a/b$ to 1. If $a/b < 1$, then $r(x)$ increases strictly monotonically from $r(0) = a/b$ to 1.*

Applying the Lemma repeatedly to the terms in equation (4), and recalling the background assumptions, we see that

$$\frac{k_C+m'}{k_D+m'} > \frac{k_C}{k_D} \quad\text{and}\quad \frac{(k_D+m')l'_D+m'k'_D}{(k_C+m')l'_C+m'k'_C} > 1\,.$$

Hence, $A/B > k_C/k_D = \alpha/\beta$ and so $d\varepsilon_{eq}/dW > 0$. It follows that ε_{eq} increases strictly monotonically from ε_0 as W increases from 0.

II. DERIVATION OF EQUATION (5) OF THE MAIN TEXT

The non-equilibrium error fraction in equation (1) can be rewritten as $\varepsilon(m') = u(m')v(m')$, where

$$u(m') = \frac{[l'_D k_D + (l'_D+k'_D)m']}{[l'_C k_C + (l'_C+k'_C)m']}\,,\text{ and}$$

$$v(m') = \frac{[k_C(l_C+m+W)+(l_C+W)m']}{[k_D(l_D+m+W)+(l_D+W)m']}\,.$$

Using the background assumptions and the Lemma, we see that, as m' increases, $u(m')$ decreases hyperbolically from $u(0) = k_D/k_C = \varepsilon_0^{-1}$ to 1 while $v(m')$ increases hyperbolically between

$$v(0) = \varepsilon_0\left(\frac{l_C+m+W}{l_D+m+W}\right) \text{ and } v(\infty) = \left(\frac{l_C+W}{l_D+W}\right)\,.$$

* Corresponding author: jeremy@hms.harvard.edu

Hence, $\varepsilon(0) = (l_C + m + W)/(l_D + m + W)$ and $\varepsilon(m') \to (l_C + W)/(l_D + W)$ as $m' \to \infty$. Furthermore,

$$\varepsilon(m') > v(0) = \varepsilon_0 \left(\frac{l_C + m + W}{l_D + m + W} \right) > \varepsilon_0^2 \,, \qquad (5)$$

as required for equation (5) in the main text.

III. THE LIMITING ARGUMENT IN KINETIC PROOFREADING

The argument for kinetic proofreading given by Hopfield [2] is based on the non-dimensional quantities,

$$\delta_1 = \frac{l'_D(m' + k_D)}{m' k'_D} \;,\; \delta_2 = \frac{m'}{k_C} \;,\; \delta_3 = \frac{m}{l_D} \;,\; \delta_4 = \frac{W}{l_D} \,,$$

which are to be taken very small. Accordingly, we consider the non-equilibrium error-fraction, ε, as defined in equation (1), in the limit as these four quantities $\to 0$. Since $k_D > k_C$, we have that

$$\delta_1 > \frac{l'_C(m' + k_C)}{m' k'_C} > 0 \,. \qquad (6)$$

If we now divide above and below by $m'k'_D = m'k'_C$ in the expression $\varepsilon = uv$ introduced above, we get

$$\varepsilon = \left(\frac{\delta_1 + 1}{l'_C(m' + k_C)/m'k'_C + 1} \right) v \,.$$

If we take $\delta_1 \to 0$ and formally treat v as a constant, we see from equation (6) that $\varepsilon \to v$ as $\delta_1 \to 0$. However, the expression for δ_1 involves m' and this is also a parameter in v. Hence, v is not constant during the limiting process, which has coupled m' to the values of the other parameters. If we ignore this coupling, we can divide above and below in v by k_C to get

$$v = \frac{(1 + \delta_2)(W + l_C) + m}{(k_D/k_C + \delta_2)(W + l_D) + m k_D/k_C}$$

and if then let $\delta_2 \to 0$, we see that

$$v \to \varepsilon_0 \left(\frac{W + l_C + m}{W + l_D + m} \right) \,.$$

If we now divide above and below in this expression by l_D, we get

$$\frac{W/l_D + l_C/l_D + m/l_D}{W/l_D + 1 + m/l_D} \to \varepsilon_0^2$$

as $\delta_3 \to 0$ and $\delta_4 \to 0$. Hence, putting the sequence of limits together, we have, formally,

$$\lim_{\delta_4 \to 0} \lim_{\delta_3 \to 0} \lim_{\delta_2 \to 0} \lim_{\delta_1 \to 0} \varepsilon = \varepsilon_0^2 \,.$$

This seems to be the interpretation that has been given in the literature to Hopfield's assertion that kinetic proofreading achieves the error fraction of ε_0^2.

The coupling noted above specifically affects m', which has to satisfy two conditions. On the one hand m' has to be large, in order that u should be close to $u(\infty) = 1$. That is the role of $\delta_1 \to 0$. On the other hand m' has to be small, in order that v should be close to $v(0)$. That is the role of $\delta_2 \to 0$. The remaining limits for δ_3 and δ_4 are only there to make sure that $v(0) \to \varepsilon_0^2$; compare equation (5). The consequence of the coupling between the δ_1 and δ_2 limits, which arises through m', can be seen by rewriting δ_1,

$$\delta_1 = \left(\frac{l'_D}{k'_D} \right) \left(1 + \left(\frac{k_D}{k_C} \right) \frac{1}{\delta_2} \right) \,.$$

Hence, in the limit as $\delta_1 \to 0$ and $\delta_2 \to 0$,

$$\frac{l'_D}{k'_D} = \frac{l'_C}{k'_C} \to 0 \,.$$

In order to achieve the proofreading limit, it is necessary for rates other than m' to change. Specifically, the "on rates" for the first discrimination, $k'_C = k'_D$, must become large with respect to those for the second discrimination, $l'_C = l'_D$.

IV. DERIVATION OF EQUATION (7) OF THE MAIN TEXT

Suppose that $R(x)$ and $Q(x)$ are allowable functions, as defined in the main text, with $R(x)/x^\alpha \to c_1$ and $Q(x)/x^\beta \to c_2$, as $x \to \infty$, where $c_1, c_2 > 0$.

Since $R^{-1}/x^{-\alpha} \to (c_1)^{-1} > 0$, it follows that R^{-1} is allowable and $\deg(R^{-1}) = -\deg(R)$. Since $(RQ)/x^{\alpha+\beta} \to c_1 c_2 > 0$, it follows that RQ is allowable and $\deg(RQ) = \deg(R) + \deg(Q)$. Finally, suppose, without loss of generality, that $\max(\alpha, \beta) = \alpha$, so that $\alpha \geq \beta$. Then,

$$\frac{R + Q}{x^\alpha} = \left(\frac{R}{x^\alpha} \right) + \left(\frac{Q}{x^\beta} \right) x^{\beta - \alpha} \,. \qquad (7)$$

The limit of this, as $x \to \infty$, is $c_1 > 0$, if $\alpha > \beta$, or $c_1 + c_2 > 0$, if $\alpha = \beta$. In either case, the limit is positive. Hence, $R + Q$ is allowable and $\deg(R + Q) = \max(\deg(R), \deg(Q))$. This proves equation (7) of the main text.

V. DERIVATION OF EQUATION (14) OF THE MAIN TEXT

Suppose that $S(x)$ is an allowable function and that $S/x^\alpha \to c > 0$, where $\alpha = \deg(S)$. Since $\ln$ is a continuous function,

$$\ln(S(x)) - \alpha \ln(x) \to \ln(c) \,.$$

Dividing through by $\ln(x)$, we see that

$$\frac{\ln(S(x))}{\ln(x)} \to \alpha \,. \qquad (8)$$

If $\deg(S) = \alpha > 0$, then $\ln(S) \sim \ln(x)$, while if $\deg(S) < 0$ then $\ln(S) \sim \ln(x^{-1})$, which proves equation (14) of the main text.

VI. DERIVATION OF EQUATION (15) OF THE MAIN TEXT

Note that if $R(x), Q(x), S(x), T(x)$ are functions, not necessarily allowable, and if $R \sim Q$ and $S \sim T$, so that $R/Q \to c_1 > 0$ and $S/T \to c_2 > 0$, then $(RS)/(QT) \to c_1 c_2 > 0$, so that $RS \sim QT$. We will use this without reference below.

Following the discussion in the main text, consider $P(i \rightleftarrows j) = (R - Q)\ln(R/Q)$ where R and Q are allowable functions with $R/x^\alpha \to c_1 > 0$ and $Q/x^\beta \to c_2 > 0$. There are three cases to consider.

Suppose that $\alpha \neq \beta$. If $\alpha > \beta$, then the same argument as in equation (7) shows that $(R - Q) \sim x^\alpha$. By equation (7) of the main text, $\deg(R/Q) > 1$, so that $\ln(R/Q) \sim \ln(x)$. Hence, $P(i \rightleftarrows j) \sim x^\alpha \ln(x)$. If $\alpha < \beta$, then $(R-Q) \sim -x^\beta$ and $\ln(R/Q) \sim -\ln(x)$, so that $P(i \rightleftarrows j) \sim x^\beta \ln(x)$. This proves case 1.

Suppose that $\alpha = \beta$ but $c_1 \neq c_2$. Then, $(R - Q)/x^\alpha \to c_1 - c_2 \neq 0$. Also,

$$\frac{R}{Q} = \left(\frac{R}{x^\alpha}\right)\left(\frac{x^\alpha}{Q}\right) \to \frac{c_1}{c_2} > 0\,.$$

Hence, $\ln(R/Q) \to \ln(c_1/c_2)$. Since $(c_1 - c_2)\ln(c_1/c_2) > 0$, it follows that $P(i \rightleftarrows j) \sim x^\alpha$, which proves case 2.

Suppose that $\alpha = \beta$ and $c_1 = c_2$. Then $(R - Q)/x^\alpha \to 0$ and $R/Q \to 1$, so that $\ln(R/Q) \to 0$. Hence, $P(i \rightleftarrows j)/x^\alpha \to 0$ as $x \to \infty$, so that $P(i \rightleftarrows j) \prec x^\alpha$, which proves case 3.

VII. DERIVATION OF EQUATION (20) OF THE MAIN TEXT

For the Hopfield mechanism (Fig. 1(a) of the main text), we described in the main text how the asymptotic error rate of $\varepsilon \sim x^{-2}$ could be achieved, by assuming that the labels are allowable functions of x such that: $\deg(l'_D) = \deg(l'_C) = -1$, $\deg(k_D) = \deg(l_D) = 1$ and $\deg(k'_C) = \deg(k_C) = \deg(k'_D) = \deg(m') = \deg(m) = \deg(l_C) = \deg(W) = 0$. Using equations (1) and (3) of the main text, we find that $\deg(p_1^*) = \deg(p_{2_C}^*) = \deg(p_{3_C}^*) = 0$, $\deg(p_{2_D}^*) = -1$, and $\deg(p_{3_D}^*) = -2$. It is helpful to introduce the notation $R \approx Q$, for functions $R(x), Q(x)$ which may not be allowable, to signify that $\lim_{x\to\infty} R/Q = 1$. We can use this to calculate the asymptotic behaviour of the terms $P(i \rightleftarrows j)$ in the entropy production rate (equation (12) of the main text). For instance,

$$P(1 \rightleftarrows 3_C) = ((l_C + W)p_{3_C}^* - l'_C p_1^*)\ln\left(\frac{(l_C + W)p_{3_C}^*}{l'_C p_1^*}\right),$$

The only term in this expression which depends on x is l'_C for which $\deg(l'_C) = -1$. Since $\deg(\ln(R)) \approx \deg(R)\ln(x)$ (equation (8)), it follows that

$$P(1 \rightleftarrows 3_C) \approx (l_C + W)p_{3_C}^* \ln(x)\,.$$

Similar calculations yield $P(2_C \rightleftarrows 3_C) \approx C_1, P(1_C \rightleftarrows 2_C) \approx C_2, P(1 \rightleftarrows 3_D) \lesssim C_3, P(2_D \rightleftarrows 3_D) \lesssim C_4$, and $P(1_D \rightleftarrows 2_D) \approx C_5$, where C_1, C_2, C_3, C_4, and C_5 are constants independent of x. Since $\deg(\varepsilon) = -2$, $\ln(x) \approx \ln(\varepsilon^{-1})/2$. Hence,

$$P \approx \frac{(l_C + W)}{2} p_{3_C}^* \ln(\varepsilon^{-1})\,,$$

so that

$$\lim_{x\to\infty} \frac{P}{\sigma \ln(\varepsilon^{-1})} = \frac{l_C + W}{2W}. \tag{9}$$

This proves equation (20) of the main text.

VIII. ADDITIONAL NUMERICAL CALCULATIONS

In Supplementary Figs. 1 and 2, we consider two discrimination mechanisms under the assumptions of equations (21) and (22) of the main text. Supplementary Fig. 1(a) shows a graph for McKeithan's T-cell receptor mechanism [3], while Supplementary Fig. 2(a) shows a graph different from both this and the Hopfield example. We used previously developed, freely-available software [4] to compute the Matrix-Tree formula (equation (1) of the main text) for each mechanism, from which we obtained symbolic expressions for P, ε, and σ. The graphs in Supplementary Figs. 1(a) and 2(a) have 441 and 64 spanning trees rooted at each vertex, respectively, underscoring the combinatorial complexity which arises away from equilibrium (main text, Discussion). (If a graph has reversible edges, so that $i \to j$ if, and only if, $j \to i$, which is the case for all the graphs discussed here, there is a bijection between the sets of spanning trees rooted at any pair of distinct vertices.) Supplementary Figs. 1(b)-(c) and 2(b)-(c) show numerical plots undertaken in a similar way to those for the Hopfield mechanism (main text, Fig. 2), as described in the main text. Similar vertical and diagonal bounds were found for the symmetric cases, while similar observations regarding the asymmetric cases as those made in the main text apply.

IX. ASYMPTOTIC RELATION FOR A NON-DISSOCIATION-BASED MECHANISM

We consider a discrimination mechanism having the graph shown in Supplementary Fig. 3(a). Its structure is identical to that of the Hopfield mechanism (Fig. 1(a) of the main text) but its labels differ to reflect the energy landscape illustrated in Supplementary Fig. 3(b). If the labels are allowable functions with $\deg(l'_D) = -1$ and $\deg(l'_C) = \deg(l_C) = \deg(l_D) = 0$, then, if the mechanism reaches thermodynamic equilibrium, it follows from equation (9) of the main text that its equilibrium error fraction satisfies

$$\varepsilon_{eq} \sim x^{-1}\,. \tag{10}$$

If it is further assumed that $\deg(m'_D) = \deg(m'_C) = -1$ and $\deg(m_D) = -\deg(m_C) = 1/2$, while all other labels have degree 0, then the mechanism is no longer at equilibrium. Using equations (1) and (3) of the main text, we find that

$$\begin{aligned}
\rho_1 &= [(m'_C+k)(l_C+W)+km_C][(m'_D+k)(l_D+W)+km_D] \\
\rho_{2_C} &= [m_C(l'_C+k')+k'(l_C+W)][(m'_D+k)(l_D+W)+km_D] \\
\rho_{3_C} &= [m'_C(k'+l'_C)+kl'_C][(k+m'_D)(l_D+W)+m_Dk] \\
\rho_{2_D} &= [(m'_C+k)(l_C+W)+km_C][m_D(l'_D+k')+k'(l_D+W)] \\
\rho_{3_D} &= [m'_D(k'+l'_D)+kl'_D][(k+m'_C)(l_C+W)+m_Ck]\,.
\end{aligned}$$

It follows that

$$\deg(p_1^*) = \deg(p_{2_C}^*) = \deg(p_{3_C}^*) = \deg(p_{2_D}^*) = 0 \quad (11)$$

and that

$$\deg(p_{3_D}^*) = -3/2, \quad (12)$$

Using equations (7) and (14) of the main text along with equations (11) and (12), we can calculate the asymptotics of the terms in the entropy production rate P (equation (12) of the main text), assuming, as in the proof of the Theorem, that we are outside the measure-zero subset of parameter space arising from case 3 of equation (15) of the main text. We find that

$$\begin{aligned}
P(1 \rightleftarrows 2_C) &\sim 1 \\
P(2_C \rightleftarrows 3_C) &\sim x^{-1/2}\ln(x) \\
P(1 \rightleftarrows 3_C) &\sim 1 \\
P(1 \rightleftarrows 2_D) &\sim 1 \\
P(2_D \rightleftarrows 3_D) &\sim x^{-1}\ln(x) \\
P(1 \rightleftarrows 3_D) &\sim x^{-1}\ln(x).
\end{aligned}$$

It follows that $P \precsim 1$, so that the entropy production rate is asymptotically constant or vanishes. Furthermore, it can be shown from equations (11) and (12) that $\deg(\varepsilon) = -3/2$ and $\deg(\sigma) = 0$. Hence, the error rate is asymptotically better than at equilibrium, for which $\deg(\varepsilon_{eq}) = -1$ (equation (10)), while the speed remains asymptotically constant. This reflects a different asymptotic relation to that in equation (19) of the main text.

[1] Gunawardena, J. *A linear framework for time-scale separation in nonlinear biochemical systems*, PLoS ONE **7**, e36321 (2012).

[2] Hopfield, J. J. *Kinetic proofreading: a new mechanism for reducing errors in biosynthetic processes requiring high specificity*, Proc. Natl. Acad. Sci. USA **71**, 4135 (1974).

[3] McKeithan, T. W. *Kinetic proofreading in T-cell receptor signal transduction*, Proc. Natl. Acad. Sci. USA **92**, 5042 (1995).

[4] Ahsendorf, T., Wong, F., Eils, R. & Gunawardena, J. *A framework for modelling gene regulation which accommodates non-equilibrium mechanisms*, BMC Biol. **12**, 102 (2014).

[5] Banerjee, K., Kolomeisky, A. B. and Igoshin, O. A. *Elucidating interplay of speed and accuracy in biological error correction*, Proc. Natl. Acad. Sci. USA **114**, 5183 (2017).

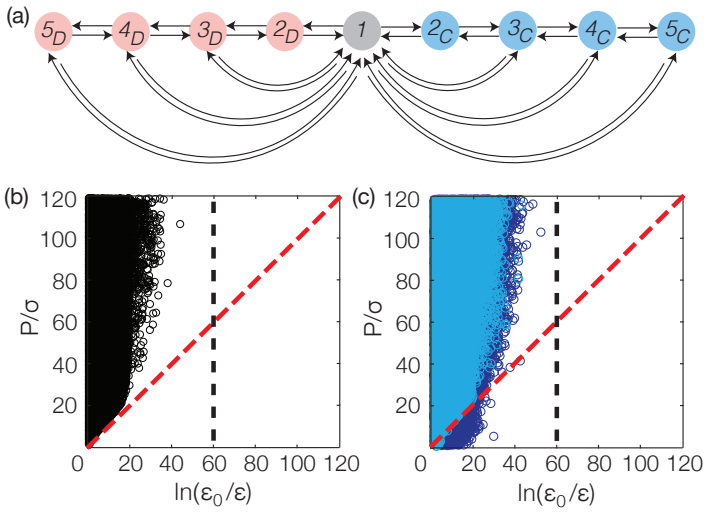

FIG. 1. Numerics for the T-cell receptor mechanism. (a) Graph for an instance of McKeithan's T-cell receptor mechanism [3], with label names omitted for clarity. (b) Plot of P/σ against $\ln(\varepsilon_0/\varepsilon)$ for approximately 10^5 points, with the labels satisfying equations (21) and (22) of the main text and numerically sampled as described in the main text. The vertical black dashed line corresponds to the bound $\varepsilon > \varepsilon_0^4$ for this mechanism (calculation not shown) that is analogous to equation (5) of the main text for the Hopfield mechanism. The diagonal red dashed line corresponds to equation (23) of the main text, as discussed further there. (c) Similar plot to (b) but with internal discrimination between correct and incorrect substrates, as described in the text, with the light blue points having a lower asymmetry range ($A = 1$) and the dark blue points having a higher range ($A = 5$).

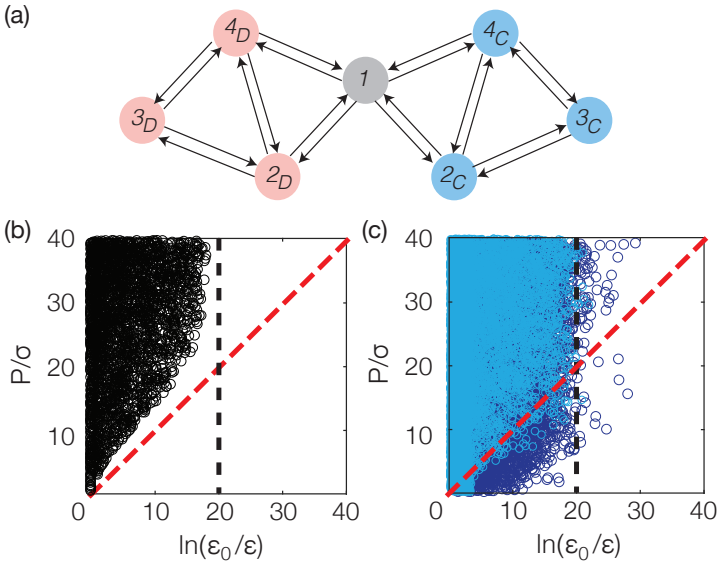

FIG. 2. Numerics for another discrimination mechanism. (a) Graph for a discrimination mechanism that is different from both the Hopfield and McKeithan mechanisms, with label names omitted for clarity. (b) Points plotted as in Supplementary Fig. 1(b). The vertical black dashed line corresponds to the bound $\varepsilon > \varepsilon_0^2$ for this mechanism (calculation not shown) that is analogous to equation (5) of the main text for the Hopfield mechanism. The diagonal red dashed line corresponds to equation (23) of the main text, as discussed further there. (c) Similar plot to (b) but with internal discrimination between correct and incorrect substrates, as described in the text, with the light blue points having a lower asymmetry range ($A = 1$) and the dark blue points having a higher range ($A = 5$).

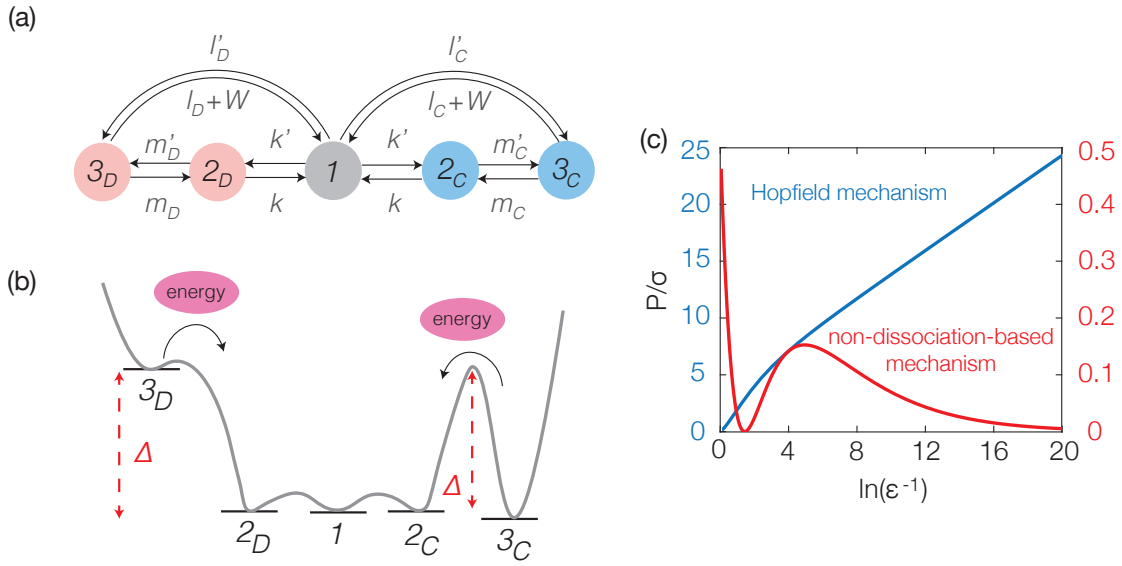

FIG. 3. A non-dissociation-based mechanism. (a) Graph with the same structure as that for the Hopfield mechanism (Fig. 1(a) of the main text) but no discrimination between C and D takes place through $1 \rightleftarrows 2_X$, while internal discrimination takes place through $2_X \rightleftarrows 3_X$, as reflected in the label names. (b) Hypothetical energy landscape for the mechanism shown in (a), illustrating where energy may be expended to drive the steps with labels m_C and m_D. (c) Plot of P/σ against $\ln(\varepsilon^{-1})$ for a numerical instance of the Hopfield mechanism (Fig. 1(a) of the main text, in blue) and a numerical instance of the non-dissociation-based mechanism in (a) (in red), as x is varied in the range $x \in [0, e^{20}]$. The numerical label values have been determined by taking $k_D = l_D = x$ and $l'_C = l'_D = x^{-1}$ for the Hopfield mechanism and $l'_D = m'_D = m'_C = x^{-1}$, $m_D = x^{1/2}$ and $m_C = x^{-1/2}$ for the non-dissociation-based mechanism, with all other labels being 1.

label	DNAP	ribosome (wild type)	ribosome (hyperaccurate)	ribosome (error-prone)
k_C	900	0.5	0.41	0.43
k_D	900	47	46.002	3.999
k'_C	0.001	40	27	37
k'_D	0.0092	27	25.002	36.001
m_C	0.2	0.001	0.001	0.001
m_D	2.3	$[4.5 \times 10^{-8}, 21.9]; 10^{-7}$	$[6.0 \times 10^{-8}, 16.6]; 10^{-7}$	$[4.7 \times 10^{-8}, 17.5]; 10^{-7}$
m'_C	700	25	14	31
m'_D	700	1.2	0.49	3.906
l_C	1	0.085	0.048	0.077
l_D	1×10^{-5}	0.6715	0.4963	0.5891
l'_C	250	0.001	0.001	0.001
l'_D	0.002	$[1.7 \times 10^{-10}, 0.06]; 0.0272$	$[1.8 \times 10^{-10}, 0.05]; 0.0299$	$[5.8 \times 10^{-9}, 2.1]; 1.0085$
W_C	250	8.415	4.752	7.623
W_D	0.012	0.0353	0.0035	0.0313

TABLE I. Experimentally measured parameter values, in units of s^{-1}, for the Hopfield mechanism in Fig. 1(a) of the main text, shown for discrimination during DNA replication by the bacteriophage T7 DNA polymerase (DNAP) and discrimination during mRNA translation by three *E. coli* ribosome variants, as annotated. The values were obtained from Tables S1-S4 of [5]. The labels in the first column correspond to those in Fig. 1(a) of the main text, except that m, m' and W now have subscripts C and D, for the correct and incorrect substrates, respectively, to allow for internal discrimination, as explained in the main text. The values of m_D and l'_D were not known for the ribosome variants, so we chose m_D from m_C by randomly selecting $\ln(m_D/m_C)$ from the uniform distribution on $[-10, 10]$, which is similar to the asymmetry ranges of the other parameters, and chose l'_D to satisfy the external chemical potential constraint used by [5], as explained in footnote [45] of the main text. The intervals given for m_D and l'_D indicate the range of sampled values. Some samples have $\varepsilon < \varepsilon_0$ and these are not shown in Fig. 2(b) of the main text. The values following each interval give the averages of the plotted values in Fig. 2(b) of the main text, as indicated there by asterisks, *.